



# A novel antitumour strategy using bidirectional autophagic vesicles accumulation via initiative induction and the terminal restraint of autophagic flux

Yang Wang, Xiaowei Tai, Li Zhang, Yayuan Liu, Huile Gao, Jiantao Chen, Kairong Shi, Qianyu Zhang, Zhirong Zhang, Qin He \*

Key Laboratory of Drug Targeting and Drug Delivery Systems, West China School of Pharmacy, and State Key Laboratory of Biotherapy/Collaborative Innovation Center for Biotherapy, West China Hospital, Sichuan University, Chengdu, 610041, China

## ARTICLE INFO

### Article history:

Received 13 October 2014  
Accepted 8 December 2014  
Available online 10 December 2014

### Keywords:

Autophagic vesicles  
Bidirectional accumulation  
Anti-tumour  
TAT–Beclin 1  
HCQ liposomes

## ABSTRACT

Autophagy is a lysosomal degradation pathway that protects cancer cells from multiple endogenous and exogenous stresses, particularly during the pathogenesis of cancer. An autophagic balance exists in the tumour micro-environment. Appropriate disturbance to this balance may have therapeutic potential. Here, we report a novel antitumour strategy based on an autophagic catastrophic vacuolisation effect in tumour cells. We achieved this effect via initiative induction and the terminal restraint of autophagic flux. The TAT–Beclin 1 peptide (T–B) was constructed for the initiative induction of autophagic flux, whereas hydroxychloroquine (HCQ)-loaded liposomes (HCQ-Lip) were constructed for terminal restraint. We demonstrate that T–B, a new CPP tandem autophagy inducing peptide, effectively activates the autophagy signal at the early stage of the autophagy pathway. HCQ deacidified the lysosome during the final stage of autophagy. We combined T–B and HCQ-Lip to induce autophagic catastrophic vacuolisation and death in several tumour cell lines based on the idea of “broadening sources of income and reducing expenditure”. The co-treated group exhibited at least a 1.86-fold greater and up to 5.66-fold greater cytotoxic effect in vitro. In addition, this strategy showed at least a 2.0-fold tumour inhibitory effect compared to the other groups in vivo. Therefore, this bidirectional accumulation of autophagic vesicles exhibited potential efficacy for tumour treatment.

© 2014 Elsevier B.V. All rights reserved.

## 1. Introduction

Macroautophagy (referred to here as ‘autophagy’) is an intracellular, bulk degradation process in which a portion of the cytoplasm is sequestered in an autophagosome and subsequently degraded upon fusion with a lysosome [1,2]. This pathway allows cells to degrade a portion of their own proteins and organelles to maintain the cellular homeostasis required for normal growth, development and adaption to stress [3]. Degradation of the sequestered material generates nucleotides, amino acids, and free fatty acids that are recycled for macromolecular synthesis and ATP generation [4]. Under normal physiological conditions, autophagy in cells or tissues occurs at low basal levels, which is primarily controlled by the serine/threonine protein kinase mammalian target of rapamycin (mTOR) [5]. However, autophagy levels in cells change when the nutritional status, hormonal factors, and other factors, such as temperature, oxygen concentration and cell density, fluctuate [2,6]. Autophagy is closely associated with human

disease and physiology. Deregulation of autophagy is implicated in multiple degenerative diseases, ageing, microbial infection and cancer [5]. Paradoxically, autophagy can protect cells but may also contribute to cell damage [7]. The exact roles of autophagy in different disease processes require further investigation (Fig. 1).

In cancer, autophagy may function in both the promotion and prevention of tumour progression [8]. A defect in autophagy may be a potentially oncogenic event but may recur during later states of tumour progression, thereby allowing the tumour cells to overcome endogenous stress, such as hypoxia, and increasing chemotherapy or radiotherapy resistance [9]. Therefore, recent studies have investigated the selective modulation of autophagy at different stages of tumour progression [10]. In addition, combination treatment of chemotherapy or radiotherapy with autophagic modulators has garnered extensive attention worldwide [5].

In mammalian cells, the primary signalling pathways regulating autophagy are controlled upstream by PtdIns3K–Akt–mTORC1, AMPK, p53, and the Bcl-2 protein family [11]. One of the core molecular machinery components modulating autophagy is the class III phosphatidylinositol 3-kinase complex [12,13]. Beclin 1 is conserved in this complex and plays a key role in autophagic flux [14]. Combined with

\* Corresponding author at: Key Laboratory of Drug Targeting and Drug Delivery Systems, West China School of Pharmacy, Sichuan University, Chengdu, 610041, China.

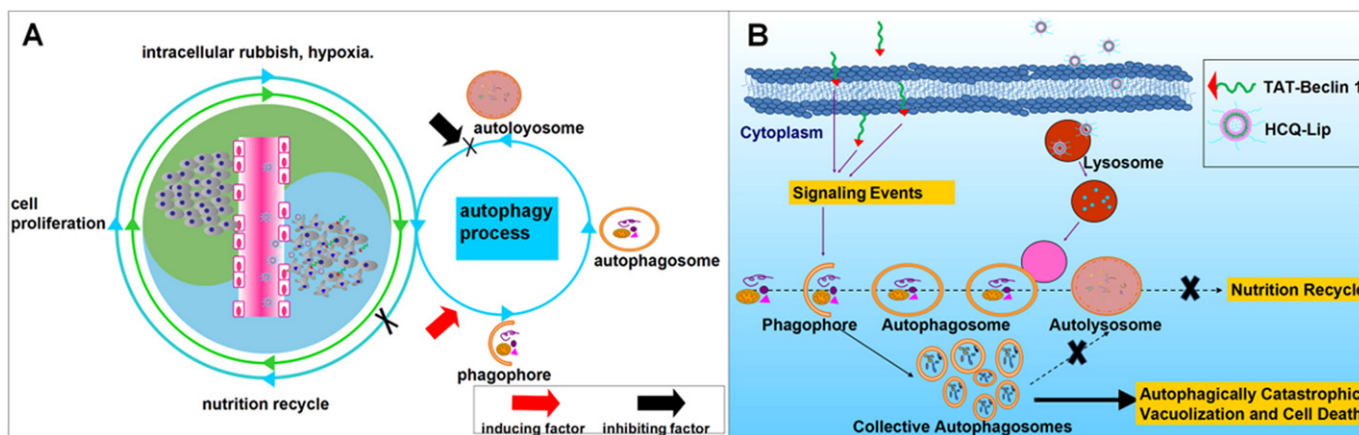


**Fig. 1.** Schematic illustration of the autophagic catastrophic vacuolisation effect for tumour suppression. (A) The autophagic balance in the tumour microenvironment (green cycle). Our intervention in this balance (blue cycle) is performed by initiative induction (red arrow) and terminal restrain (black arrow) of the autophagic process. (B) The disturbed autophagic balance in tumour cells and cell death induced by HCQ-Lip plus T-B co-treatment.

hVps34 and p150, Beclin 1 performs its autophagy-inducing function following downstream signalling cascades [15]. By contrast, the binding of Bcl-2 protein family members, such as Bcl-2 and Bcl-X<sub>L</sub>, to Beclin 1 via the BH3 domain within Beclin 1 disrupts Beclin 1 binding to hVps34 and p150 and impairs Beclin 1-associated hVps34 PtdIns3K activity, thereby inhibiting autophagic flux [8]. Malignant cells often display defects in autophagy, and the *beclin 1* gene is monoallelically deleted in 40–75% of cases of human sporadic breast, ovarian, and prostate cancer [16]. Here, we designed the TAT-Beclin 1 peptide (T-B). Functional T-B (YGRKKRRQRRRGGTNVFNATFEIWHDGEGFT) consists of the cell-penetrating peptide TAT protein transduction domain (YGRKKRRQRRR) modified with the Beclin 1 amino acids 267–284 (TNVFNATFEIWHDGEGFT) via a G2 linker. This T-B both possesses Beclin 1 biological activity and can also enter cells [17].

To achieve improved tumour suppression, we hypothesised a seemingly paradoxical strategy for autophagy modulation. We predicted an autophagic catastrophic vacuolisation effect resulting from this strategy. HCQ (hydroxychloroquine), a conventional autophagy inhibition agent, functioned at a high dosage, which is inconsistently achieved in humans [18]. Liposomes effectively accumulate in tumour and inflammation tissue via the EPR effect, which can reduce the therapeutic dose and toxicity [19]. We prepared HCQ-Lip (HCQ-loaded liposomes) to allow HCQ to target tumours. Our strategy was performed using the combined application of T-B with HCQ-Lip. Autophagy initiation-related signal events induced by T-B plus the terminal autophagy inhibitory effect of HCQ-Lip result in autophagosome accumulation, which effectively caused apoptosis and necrosis. Therefore, we report and demonstrate for the first time that a significant antitumour effect can be achieved using this autophagic catastrophic vacuolisation strategy.

## 2. Materials and methods

### 2.1. Materials

Hydroxychloroquine sulphate (H1306) was purchased from TCI Development Co., Ltd. (Shanghai, China). SPC was purchased from the Taiwei Chemical Company (Shanghai, China). Cholesterol and DSPE-PEG2000 were purchased from Avanti Polar Lipids (Alabaster, AL, USA). Anti-LC3 (PM036) was purchased from Medical & Biological Laboratories Co., Ltd. (Japan). P62/SQSTM1 polyclonal antibody (18420-1-AP) was purchased from Protein Tech Co., Ltd. (St. Louis, MO, USA). Lyso-tracker™ was purchased from Invitrogen (Carlsbad, CA, USA). The annexin V-FITC/PI apoptosis detection kit was obtained from KeyGEN Biotech (China). Plastic cell culture dishes and plates were purchased from Wuxi NEST Biotechnology Co. (Wuxi, China). Other

chemicals and reagents were of analytical grade. T-B was synthesised according to the standard solid phase peptide synthesis by Chinapeptides Co., Ltd. (Shanghai, China).

### 2.2. Preparation and characterisation of HCQ-Lip

HCQ-Lip was prepared by a transmembrane pH-gradient method including the preparation of blank long-circulation liposomes and drug loading. Blank liposome vesicles were prepared by the thin film hydration method. Briefly, SPC, cholesterol and DSPE-PEG2000 (molar ratio = 35:19:2) were dissolved in chloroform. Next, the chloroform was removed by rotary evaporation, and the film was further dried and stored under a vacuum overnight. The thin film was hydrated in 0.10 M citrate buffer (pH 3.6) for 40 min. Then, the sample was intermittently sonicated with a probe sonicator at 80 W for 75 s to form the primary blank liposomes. The pH gradient between the internal phase and the external of the blank liposomes was formed by adjusting the external phase pH with alkali to 7.2. Then, HCQ was added and incubated with pH gradient liposomes system for 15 min at 40 °C. Untrapped HCQ was removed by eluting the liposome aqueous system over a Sephadex G-50 column (1 cm × 25 cm) with PBS. The entrapment efficiency of HCQ was determined by HPLC. The particle size and zeta potentials of the HCQ liposomes were measured using a laser particle size analyser (Malvern Nano ZS, Malvern, UK).

### 2.3. Cells, LC3-GFP plasmid and eGFP-LC3-expressing cells

HepG2 cells, 4T1 cells, and HeLa cells were cultured in RPMI-1640 medium, and MCF-7 cells were cultured in DMEM, and all were supplemented with 10% FBS, 100 U/mL streptomycin, and 100 U/mL penicillin in an atmosphere of 5% CO<sub>2</sub> at 37 °C. The eGFP-LC3 plasmid was obtained from Addgene. The eGFP-LC3-expressing 4T1 cells (4T1 eGFP-LC3 cells), eGFP-LC3-expressing MCF-7 cells (MCF-7 eGFP-LC3 cells), eGFP-LC3-expressing HeLa cells (HeLa eGFP-LC3 cells) and eGFP-LC3-expressing HepG2 cells (HepG2 eGFP-LC3 cells) were constructed by eGFP-LC3 plasmid transfection. Briefly, cells were allowed to grow to 0.25–1 × 10<sup>6</sup> per single well (6-well) in 2 mL RPMI-1640 without antibiotics and were then transfected using Lipofectamine 2000 (Invitrogen, Carlsbad, California, United States) according to the manufacturer's instructions. For each well (6-well), 14 µg pooled eGFP-LC3 plasmid was diluted in 700 µL OptiMEM. After a 5-min incubation at room temperature, the diluted RNA and Lipofectamine 2000 were combined and incubated for 10 min at room temperature. The 250 µL plasmid-reagent complex was then added to the well. The eGFP-LC3-expressing cells were obtained after 24 h incubation.

#### 2.4. *In vitro* proliferation and cell viability assays

For the MTT assay, cells ( $2\text{--}5 \times 10^3$  per well) were seeded onto a 96-well plate, and five wells were included in each group. After the cells were cultured overnight, HCQ and HCQ liposomes were added. After 2 h, the TAT–Beclin 1 ( $15 \mu\text{M}$ ) was added. The incubation continued for 24 h. Next,  $20 \mu\text{L}$  MTT solution ( $5 \text{ mg/mL}$  in PBS) was added to each well and the cells were incubated for 4 h under 5%  $\text{CO}_2$  at  $37^\circ\text{C}$ . Then, the medium was replaced with  $150 \mu\text{L}$  DMSO. The absorbance at  $570 \text{ nm}$  was measured with a microplate reader (Thermo Scientific Varioskan Flash), using wells without cells as blanks.

For the apoptosis assay, an annexin V-FITC/PI double staining method was used. Cells were treated with the dosing regimen for 24 h. At the end of the treatment, the cells were trypsinised, washed with PBS and centrifuged at  $3000 \text{ rpm}$  for 5 min. Then, the cells were resuspended in  $500 \mu\text{L}$  binding buffer and stained with  $5 \mu\text{L}$  annexin V-FITC and  $5 \mu\text{L}$  PI. The cells were incubated in the dark at room temperature for 15 min. Finally, the stained cells were collected for cytometric analyses (Cytomics™ FC 500, Beckman Coulter, Miami, FL, USA).

#### 2.5. Growth inhibition of tumour spheroids

To prepare the three-dimensional tumour spheroids, 4T1 cells were seeded in 96-well plates coated with  $100 \mu\text{L}$  2% low melting point agarose ( $1 \times 10^5$  cells per well). After 6 days, the tumour spheroids were treated with PBS,  $15 \mu\text{M}$  T–B,  $50 \mu\text{M}$  HCQ, HCQ plus T–B,  $50 \mu\text{M}$  HCQ-Lip or HCQ-Lip plus T–B. Growth inhibition was monitored by measuring the size of the 4T1 tumour spheroids at days 0, 1, 3, 5, and 7. The maximal ( $d_{\text{max}}$ ) and minimal ( $d_{\text{min}}$ ) diameters of each spheroid were measured, and the spheroid volume was calculated using the following formula:  $V = (\pi \times d_{\text{max}} \times d_{\text{min}}) / 6$ . The relative 4T1 tumour spheroid volume was estimated with the following formula:  $R = (V_{\text{day } i} / V_{\text{day } 0}) \times 100\%$ , where  $V_{\text{day } i}$  is the 4T1 tumour spheroid volume at the  $i$ th day after drug application.

#### 2.6. Fluorescence imaging

For eGFP, the 4T1 eGFP–LC3 cells and MCF-7 eGFP–LC3 cells were treated and fixed with 4% (vol/vol) paraformaldehyde. For LysoTracker Red, the cells were treated with HCQ or HCQ liposomes for 1 h and labelled for 15 min with  $25 \text{ nM}$  LysoTracker Red.

Fluorescence imaging was performed using confocal microscopy procedure (TCS SP5 AOBS confocal microscopy system, Leica, Germany). To quantify autophagosome accumulation in the cells, the number of bright green puncta (autophagosomes) was counted in at least 25 cells. Three independent experiments were performed.

#### 2.7. TEM

For the cultured 4T1 cells *in vitro*, the cells were washed with PBS and then centrifuged at  $2000 \text{ rpm}$  for 5 min after drug treatment. The cell pellets were fixed in 2.5% glutaraldehyde. After fixation, the samples were post-fixed in 2% osmium tetroxide in  $0.1 \text{ mol/L}$  sodium phosphate buffer for 30 min. Ultrathin sections were then observed under a transmission electron microscope (JEOL JEM-1200EX, Japan) at  $80 \text{ kV}$ . For the 4T1, tumour tissue from the mouse model, freshly excised tissue was fixed in 2.5% glutaraldehyde, pH 7.4, for 2 h at room temperature. Then, the samples were rinsed and post-fixed. Subsequently, the tissue was dehydrated and embedded in Agar 100 resin. Nanometre sections were cut and stained. The sections were then observed under a transmission electron microscope.

#### 2.8. Morphological analysis

Approximately  $1 \times 10^5$  4T1 cells were seeded in each well of a 6-well plate overnight. Then, the drugs were added and the cells were

incubated at  $37^\circ\text{C}$  under 5%  $\text{CO}_2$  for 36 h. The cells were examined for morphological changes by inverted phase contrast microscopy (Olympus, Tokyo, Japan).

#### 2.9. Western blotting

After treatment, the cells were harvested and lysed in cell lysis buffer containing protease inhibitors. Equal amounts ( $20 \mu\text{g}$ ) of total protein were loaded onto 10% SDS-PAGE gels for separation and then transferred onto a polyvinylidene difluoride (PVDF) membrane and incubated with the specific primary antibodies at  $4^\circ\text{C}$  overnight. The membranes were washed with TBST (TBS with 0.05% Tween-20) solution. Then, the membranes were incubated with HRP-labelled secondary antibodies and detected with the Immobilon Western HRP Substrate (Millipore, USA) on a Bio-Rad ChemiDoc MP system (Bio-Rad Laboratories, USA). ImageJ was used to quantify the band intensity.

#### 2.10. Tumour xenograft experiments

BALB/C mice weighing approximately  $20 \text{ g}$  were purchased from the experimental animal centre of Sichuan University for this study. The 4T1 cells were harvested and resuspended in ice-cold PBS and s.c. injected into the left flank of mice ( $1 \times 10^6$  cells/flank) on day 0. Treatment of 4T1 tumour-bearing Balb/C mice began on the 4th day when the tumours reached  $50 \text{ mm}^3$ . The tumour-bearing mice were randomly assigned into the following four groups: PBS group, T–B group, HCQ plus T–B group, and HCQ-Lip plus T–B group. PBS and HCQ-Lip were injected through the tail vein. T–B was administered by intratumoural injection 2 h after the HCQ-Lip treatment in the HCQ plus T–B group and HCQ-Lip plus T–B group. Tumour size was measured using digital callipers, and the tumour volume was calculated using the following formula:  $\text{volume (mm}^3) = 1 / 2 A (\text{length}) \times B (\text{width})^2$ . On the 27th day of tumour inoculation, the mice were killed and the tumours were weighed and collected for evaluation.

#### 2.11. Histology and immunohistochemistry

Histological analysis of the tumour tissue and lung was performed by haematoxylin and eosin staining according to standard protocols provided by the manufacturers. Briefly,  $2\text{-}\mu\text{m}$  sections from at least three different planes of the tumours and lungs were cut and used for haematoxylin and eosin staining. Sections were evaluated using an optical microscope at various magnifications within different fields. Immunohistochemical staining was manually processed. Paraffin sections were dehydrated and antigenic epitopes were retrieved using citrate buffer ( $10 \text{ mM}$ ) and microwaving for 8 min. The sections were then incubated with primary antibodies. Peroxidase-conjugated anti-rabbit IgG was subsequently used to detect the primary Ab.

#### 2.12. Statistical analysis

If not otherwise stated, all values are presented as the means  $\pm$  SD. Statistical analysis was performed with two-tailed Student's *t*-tests for all other data. Probabilities less than 0.05 were considered significant. The red lysosomal puncta and eGFP–LC3 dot quantification was analysed using the OriginPro 8.0 Software, Origin Lab Corporation.

### 3. Results

#### 3.1. Characterisation of HCQ-Lip

HCQ-Lip was prepared using an active loading method. The particle size of HCQ-Lip was approximately  $100 \text{ nm}$  (Fig. 2A). The zeta potential of the HCQ-Lip was  $-3.96 \text{ mV}$ . The average encapsulation efficiency of the HCQ-Lip was 93.8%. The morphological characteristics of the PEG-Lip and HCQ-Lip were assessed using transmission electron microscopy

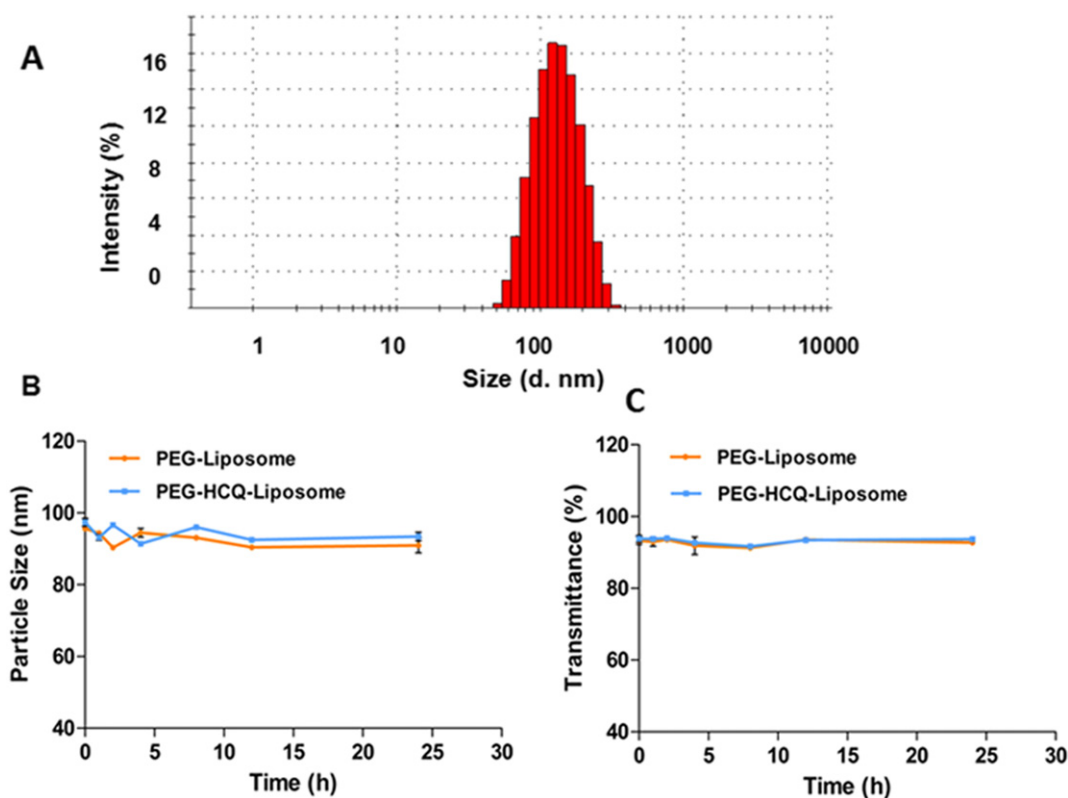


**Fig. 2.** Liposome characterisation. (A) Size distribution graph of HCQ-Lip. (B) The fluctuation in particle sizes of PEG-Lip and HCQ-Lip in 50% FBS. (C) The variations in turbidity (represented by transmittance) of PEG-Lip and HCQ-Lip in 50% FBS ( $n = 3$ , mean  $\pm$  SD).

(TEM) procedure (Fig. S1A, B) and were consistent with the size determined with a laser particle analyser. The stability of HCQ-Lip was evaluated using *in vivo* mimicking conditions. The transmittance and particle sizes did not change significantly during the 24-h incubation with 50% FBS. Fig. 2B, C shows the stability of HCQ-Lip in the presence of serum.

### 3.2. Lysosomotropic property of HCQ-Lip

HCQ is a lysosomotropic agent widely used to neutralise lysosomal pH and block lysosomal degradation [20]. To compare the lysosomotropic capacity between free HCQ and HCQ-Lip and the functional effects, 4T1 cells were treated with HCQ or HCQ-Lip at different

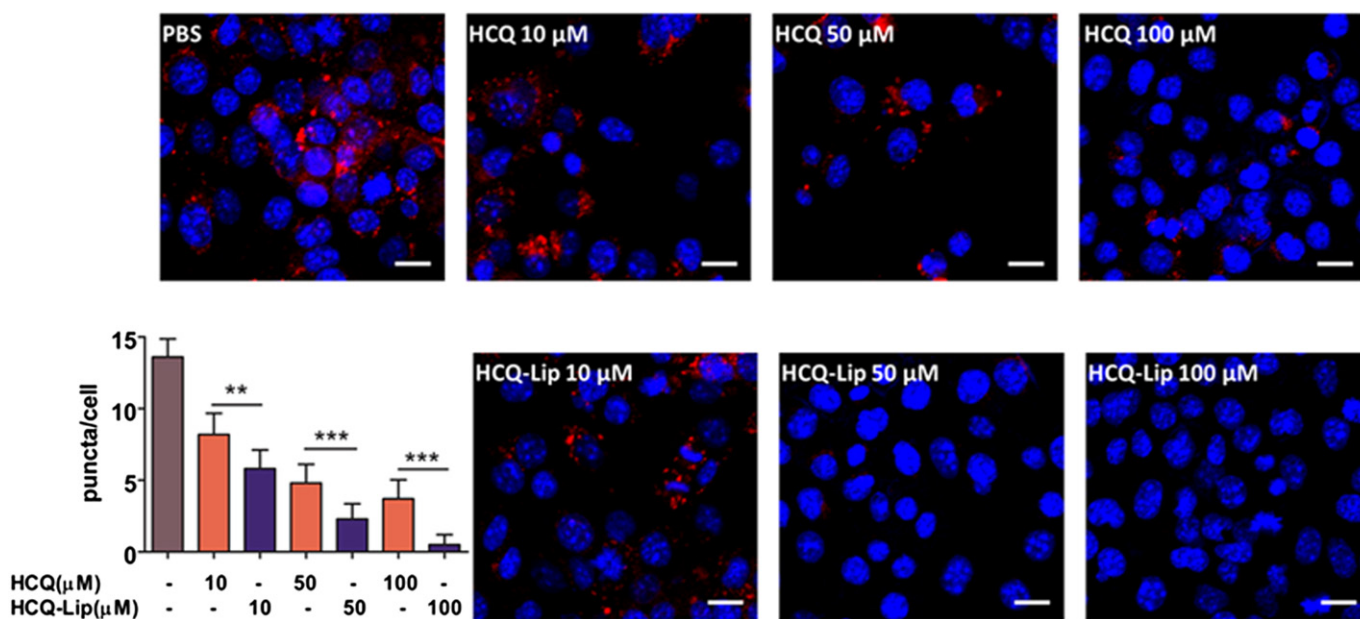


**Fig. 3.** Confocal imaging of 4T1 cells treated as indicated for 1 h and stained with LysoTracker Red. LysoTracker positive puncta (red) per cell were scored for three high-powered fields. The scale bar represents 5  $\mu$ m. Blue: nuclear DAPI staining. The data presented are the mean  $\pm$  SD. \*, \*\*, and \*\*\* indicate  $p < 0.05$ ,  $p < 0.01$ , and  $p < 0.001$  versus the compared group, respectively.

concentrations and stained with LysoTracker Red (Fig. 3). Within 1 h of treatment, fewer LysoTracker-positive puncta were observed in HCQ-Lip-treated cells than free HCQ-treated cells at both 10  $\mu$ M and 50  $\mu$ M. The results showed a 33.3% reduction of red puncta for 10  $\mu$ M HCQ-Lip vs. 10  $\mu$ M HCQ, and a 62.7% reduction of red puncta in 50  $\mu$ M HCQ-Lip vs. 50  $\mu$ M HCQ. However, when the concentration was increased to 100  $\mu$ M, there were no obvious LysoTracker-positive puncta in either group. These results show that HCQ had greater lysosomotropic potential after encapsulation in the liposomes. In addition, these data indicate that HCQ-Lip causes lysosomal dysfunction by deacidifying the

lysosome because the mechanism of LysoTracker Red staining is based on the acidity of the lysosome [21]. This lysosome deacidifying effect can lead to further impairment of the lysosomal enzymes and effective autophagy inhibition during the digestive stage of autophagic flux. Finally, our data indicate that 50  $\mu$ M HCQ-Lip effectively disrupts the internal environment of the lysosomes in vitro. There are two reasons that can explain why the HCQ-Lip have greater lysosomotropic potential than free drug. Firstly, hydroxychloroquine sulphate is highly water-soluble drug, which limits its capacity of permeating the lipid membranes of cells. After entrapment in liposomes, this problem can

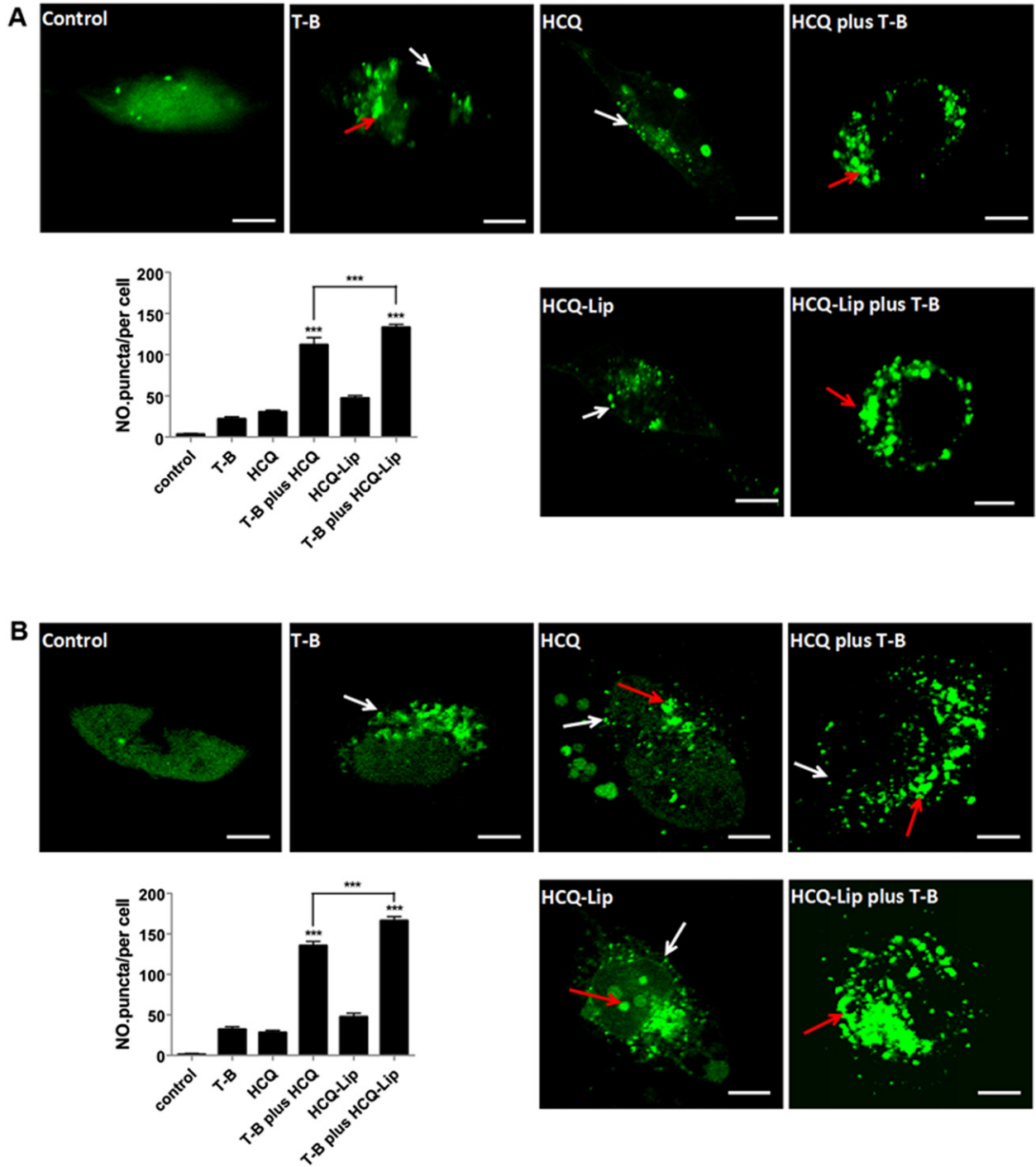


**Fig. 4.** The accumulation of autophagosomes assessed by confocal microscopy. (A) Representative images of 4T1 eGFP-LC3 cells treated as indicated for 4 h. (B) Representative images of MCF-7 eGFP-LC3 cells treated as indicated for 4 h. HCQ and HCQ-Lip were both at 50  $\mu$ M, T-B was at 15  $\mu$ M. White arrows: small puncta; red arrows: dense puncta. The scale bar represents 5  $\mu$ m. The graph shows the mean  $\pm$  SD puncta per cell. The data presented are the mean  $\pm$  SD. \*, \*\*, and \*\*\* indicate  $p < 0.05$ ,  $p < 0.01$ , and  $p < 0.001$  versus the compared group, respectively.

be eased. Secondly, liposomes are delivered into cells mainly through endocytosis and often further delivered to lysosome. Here, we made use of this pathway to delivery HCQ to lysosome, to some extent, which achieved lysosome targeting.

### 3.3. The accumulation of autophagic vesicles

To demonstrate that the autophagosome accumulation effect is induced by HCQ-Lip plus T-B co-treatment, we transfected 4T1 cells, MCF-7 cells, HepG2 cells and HeLa cells with the microtubule-associated protein 1 light chain 3 (LC3) fused to eGFP (eGFP-LC3) as previously described [22] to obtain eGFP-LC3-expressing 4T1 cells (4T1 eGFP-LC3 cells), eGFP-LC3-expressing MCF-7 cells (MCF-7 eGFP-LC3 cells), eGFP-LC3-expressing HepG2 cells (HepG2 eGFP-LC3 cells) and eGFP-LC3-expressing HeLa cells (HeLa eGFP-LC3 cells). LC3

and eGFP-LC3 localised only to the autophagic membrane structures, which indicate autophagic vesicles [23]. These four cell lines were treated with PBS as a control, and 15  $\mu$ M T-B, 50  $\mu$ M HCQ, 50  $\mu$ M HCQ plus 15  $\mu$ M T-B, and 50  $\mu$ M HCQ-Lip or 50  $\mu$ M HCQ-Lip plus 15  $\mu$ M T-B, respectively (Figs. 4A, B and S2A, B). Within 4 h of treatment, the cells treated with 15  $\mu$ M T-B showed punctate fluorescence, indicating the up-regulation of autophagic initiation. Cells treated with 50  $\mu$ M HCQ or 50  $\mu$ M HCQ-Lip exhibited analogously dense puncta, which represented terminal inhibition of autophagic flux. HCQ was always used as an autophagy inhibitor to inhibit the degradation of autophagosomes and the cargoes loaded by autophagosomes. However, the co-treated groups, including the HCQ plus T-B group and HCQ-Lip plus T-B group, produced highly dense puncta, indicating the distinct accumulation of autophagosomes. The HCQ plus T-B-treated 4T1 eGFP-LC3 cells exhibited a significant 4.80-fold increase in GFP-LC3 puncta compared

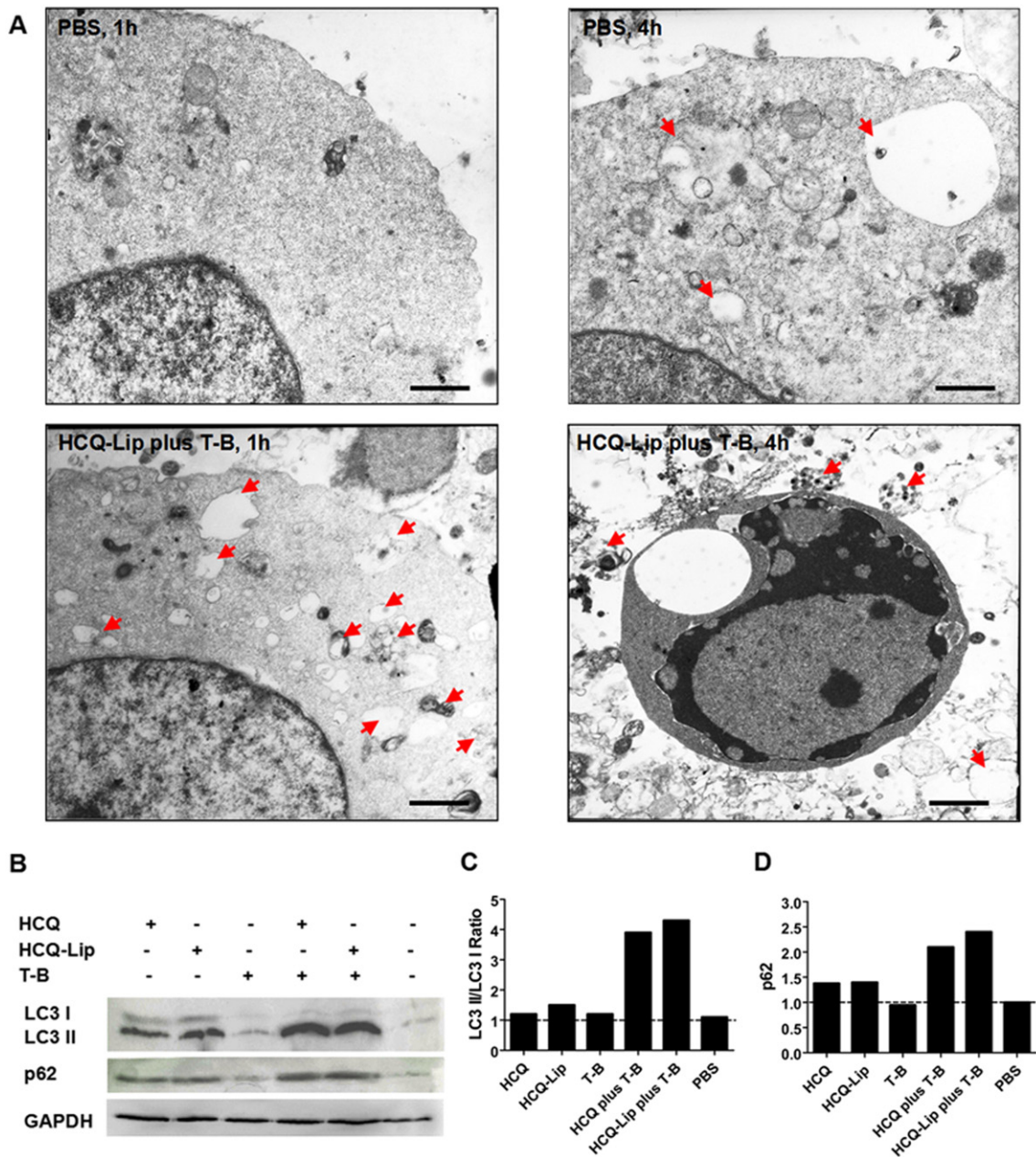


**Fig. 5.** The autophagic vacuolisation effect induced using the co-treated strategy. (A) Representative electron micrographs of 4T1 cells treated (1 h and 4 h) with PBS, or 50  $\mu$ M HCQ-Lip plus 15  $\mu$ M T-B. Arrows: autophagic vesicles. Scale bars, 500 nm. (B) LC3 and p62 Western blotting of 4T1 cells treated for 4 h as indicated with 50  $\mu$ M HCQ, 50  $\mu$ M HCQ-Lip, and 15  $\mu$ M T-B. (C) The calculated LC3II/LC3I ratios according to the results of B. (D) The calculated p62 ratios according to the result of the B vs. PBS group.

to the T-B treatment only (Fig. 4A), whereas MCF-7 eGFP-LC3 cells showed a 4.67-fold increase in GFP-LC3 puncta (Fig. 4B). Interestingly, the HCQ-Lip plus T-B group exhibited the highest number of fluorescent puncta, which was significantly different ( $p < 0.001$ ) from the HCQ plus T-B group, with a 1.27-fold increase for 4T1-eGFP-LC3 cells and a 1.35-fold increase for MCF-7 eGFP-LC3 cells. In addition, the cell morphology of the co-treated groups changed, indicating greater cell toxicity.

TEM is a valid approach for both the quantitative and qualitative analysis of autophagy. Electron micrographs of 4T1 cells treated with PBS or 50  $\mu\text{M}$  HCQ-Lip plus 15  $\mu\text{M}$  T-B showed significant morphological differences in the size and number of vesicles produced by inducing the production of new autophagic vesicles and simultaneously blocking the clearance of autophagic vesicles (Fig. 5A). After a 1-h incubation with HCQ-Lip plus T-B, the co-treated group had numerous autophagic

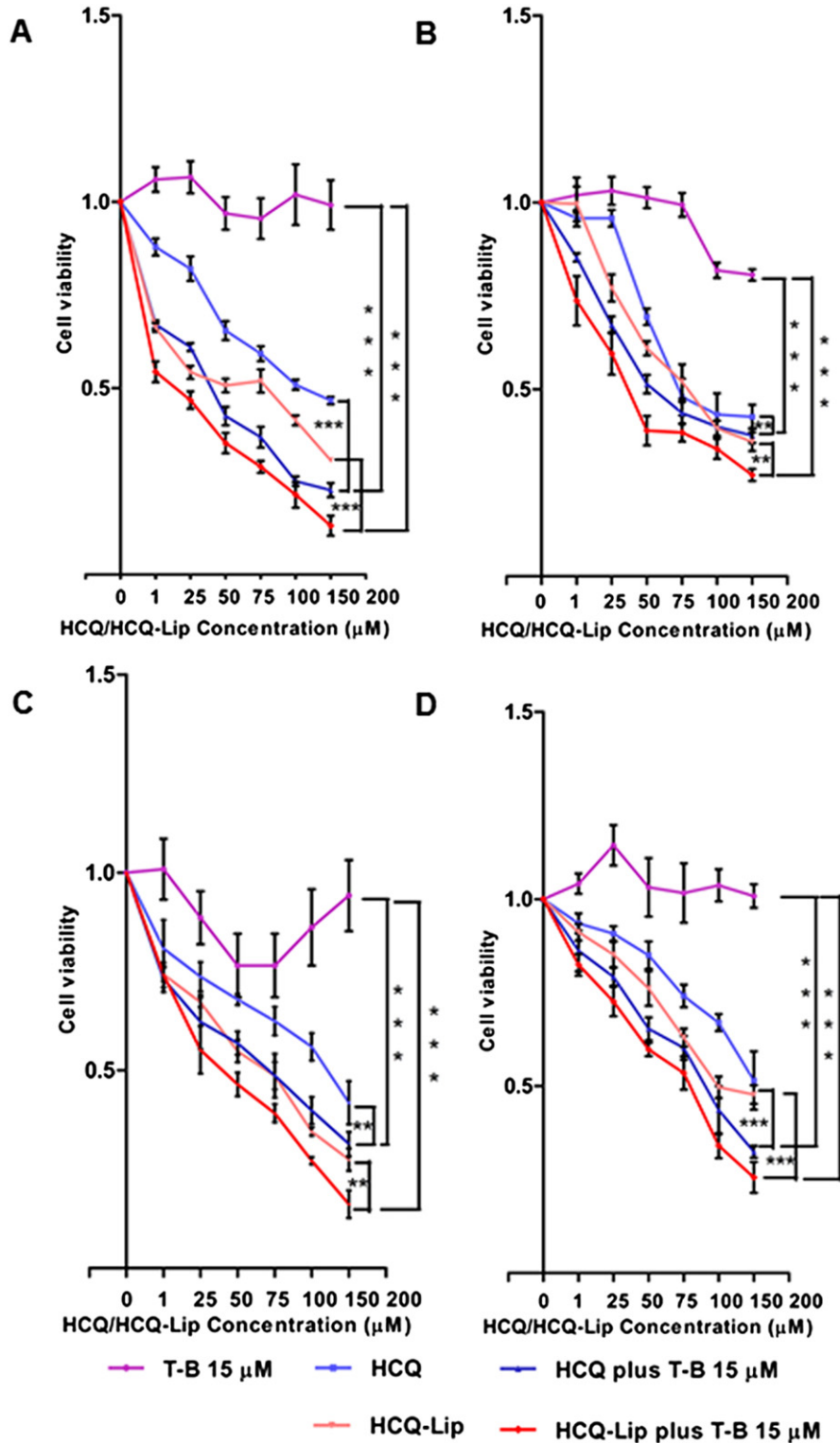


**Fig. 6.** MTT assay (24 h) for the four cancer cell lines. (A) 4T1 cell line. (B) MCF-7 cell line. (C) HepG2 cell line. (D) HeLa cell line. The values presented are the means  $\pm$  SD with five replicates per treatment. \*, \*\*, and \*\*\* indicate  $p < 0.05$ ,  $p < 0.01$ , and  $p < 0.001$  versus the control group, respectively; ns is no significance.

vesicles in the cell, whereas there were fewer in the PBS group. When the incubation was 4 h, some of the treated cells showed apoptotic features, accompanied by nuclear shrinkage and lysis (Fig. 5A).

The mammalian microtubule-associated protein 1 light chain 3 (LC3), a homologue of Apg8p in yeast, is essential for autophagy [24]. LC3 I and LC3 II are two forms of LC3 in which the former is cytosolic and the latter is membrane bound. An increase in the ratio of LC3 II/LC3 I reflects the accumulation of autophagosomes in cells [25]. LC3 Western blotting (Fig. 5B, C) demonstrated that the accumulation of autophagosomes in the co-treated group is greater than 3-fold more potent than the groups treated with T-B, free HCQ or HCQ-Lip.

The p62 protein, also called sequestosome 1, is involved in linking polyubiquitinated protein aggregates to the autophagy machinery [26]. The p62 protein is an adaptor protein involved in the delivery of ubiquitin bound cargo to the autophagosome and lysosomal degradation. When cellular autophagy is disrupted, cytoplasmic protein aggregates, including ubiquitin and p62, can be detected in a number of disease models. Inhibition of autophagy led to an increase in p62 protein levels [27,28]. Western blotting (Fig. 5B, D) showed p62 accumulation in the co-treated group, indicating disrupted autophagic flux.

These data show that autophagosomes effectively accumulate in cells after HCQ-Lip and T-B co-treatment.

### 3.4. Autophagic vacuole accumulation is cytotoxic

To determine the role of cellular vacuole accumulation for cytotoxicity, 4T1 (mice breast carcinoma), MCF-7 (human breast carcinoma), HeLa (human epidermal carcinoma), and HepG2 (human hepatic carcinoma) cells were treated with PBS as a control or free HCQ, HCQ-Lip, or T-B (15  $\mu$ M) or co-treated with HCQ plus T-B (15  $\mu$ M) or HCQ-Lip plus T-B (15  $\mu$ M) at various HCQ concentrations (1  $\mu$ M–150  $\mu$ M). The 3-(4,5-dimethylthiazol-2-yl)-2,5-diphenyltetrazolium bromide (MTT) assay was used to assess viable cells at 24 h (Fig. 6). For the four cell types tested, the co-treatment regimen of both HCQ plus T-B and HCQ-Lip plus T-B exhibited greater inhibition of cell proliferation than the free HCQ

group, T-B group and HCQ-Lip group. Furthermore, the HCQ-Lip plus T-B group displayed higher cytotoxicity than the HCQ plus T-B group, which may be because the endocytic capacity of HCQ was adjusted after liposome encapsulation. The  $IC_{50}$  of HCQ (co-treatment with 15  $\mu$ M T-B) decreased by 2.09-fold for 4T1 cells, 1.42-fold for MCF-7 cells, 1.60-fold for HepG2 cells and 1.32-fold for HeLa cells than for HCQ only. Significantly, after encapsulation in the liposomes, the  $IC_{50}$  of HCQ (co-treatment with 15  $\mu$ M T-B) decreased by 3.96-fold 4T1 for cells, 1.87-fold for MCF-7 cells, 3.84-fold for HepG2 cells and 1.53-fold for HeLa cells, compared to HCQ only (Table S1). In addition, the inhibition of *in vitro* tumour sphere growth also demonstrated the cytotoxicity of the HCQ-Lip plus T-B co-treatment (Fig. S3). These results suggest that the co-treatment strategy inducing autophagic vesicle accumulation can significantly inhibit cell proliferation, at least for these cell lines.

Mammalian cell apoptosis is accompanied by various morphological changes including cell surface changes [29]. After 24 h treatment, the apoptosis and necrosis dot diagrams of 4T1 cells treated with different regimens as indicated were consistent with the MTT results (Fig. S5). The percentage of apoptotic and necrotic cells increased by 5.66-fold (HCQ-Lip plus T-B vs. control), 3.47-fold (HCQ-Lip plus T-B vs. T-B), 1.86-fold (HCQ-Lip plus T-B vs. HCQ) and 1.55-fold (HCQ-Lip plus T-B vs. HCQ-Lip). Similarly, the HCQ-Lip plus T-B co-treated group showed greater apoptosis and necrosis induction than the HCQ plus T-B co-treated group (1.33-fold increase). MCF-7 cells had similar results 24 h after treatment, and the late apoptotic cells increased by 1.5-fold (HCQ plus T-B vs. HCQ) and 1.8-fold (HCQ-Lip plus T-B vs. HCQ-Lip) (Fig. S6A, B, E). Compared to the other groups, the HCQ plus T-B and HCQ-Lip plus T-B co-treated groups both caused cell shrinkage, rounding, membrane blebbing, cytoplasmic condensation, and detachment from the surface of the cell culture dish (Fig. S4). After 48 h treatment, the percentage of apoptotic and necrotic cells increased by 23.25-fold (HCQ-Lip plus T-B vs. control), 5.22-fold (HCQ-Lip plus T-B vs. T-B), 2.85-fold (HCQ-Lip plus T-B vs. HCQ) and 1.71-fold (HCQ-Lip plus T-B vs. HCQ-Lip). Similarly, the HCQ-Lip plus T-B co-treated group showed greater apoptosis and necrosis induction than the HCQ plus

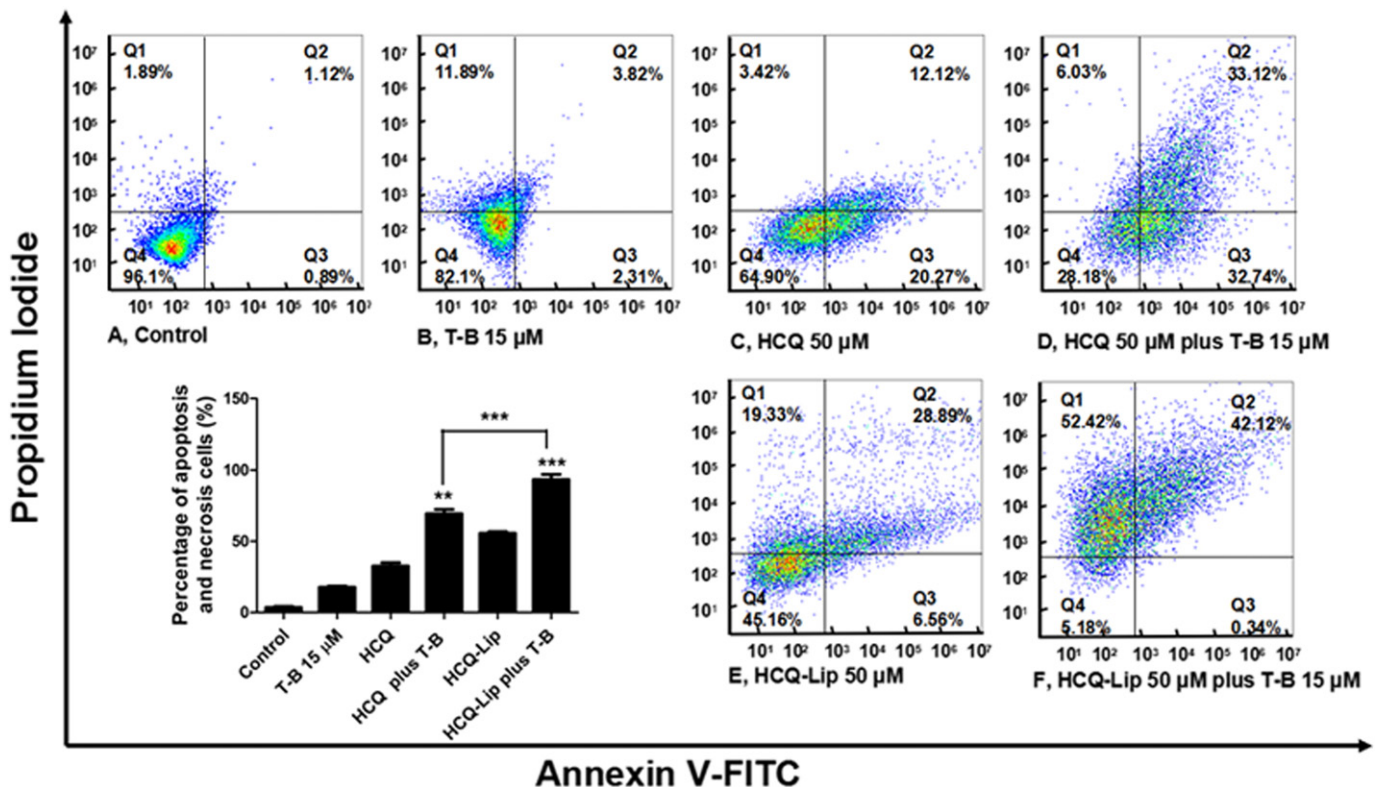


Fig. 7. Apoptosis assay of 4T1 cells after treatment as indicated for 48 h. The values presented are the means  $\pm$  SD ( $n = 3$ ). \*\*\* indicates  $p < 0.001$  versus the compared group.

T–B co-treated group (1.36-fold increase) (Fig. 7). These studies indicate that increased autophagic vacuole accumulation results in apoptosis and necrosis.

### 3.5. In vivo antitumour efficiency

To evaluate the antitumour efficiency of autophagosome accumulation in vivo, 4T1 xenograft-bearing BALB/C mice were established. Six mice bearing 4T1 xenografts per group were treated with PBS, T–B (1.5 mg/kg), HCQ (65 mg/kg) plus T–B (1.5 mg/kg), or HCQ-Lip (65 mg/kg) plus T–B (1.5 mg/kg) and dosed for 2 days with daily treatment with 2 days off treatment (2/4 days) for all four treatment groups to allow for symptom recovery and to avoid excess toxicity. PBS, HCQ and HCQ-Lip were administered by intravenous injection, whereas T–B was administered by intra-tumoural injection. Compared to the rapid growth in tumour volume for the PBS group, the other three groups all exhibited varying degrees of tumour inhibition (Fig. 8A). The HCQ-Lip exhibited greater antitumour efficiency than the free HCQ, which may be caused by the EPR effect of PEGylated HCQ liposomes. The EPR effect effectively improves the distribution of HCQ in tumours. The tumour therapeutic effect of T–B was first shown in our study. T–B treatment showed an 18.4% reduction of the average daily tumour growth rate vs. the control group and a 63% reduction of excised tumour weight after 27 days of therapy vs. the control group. Beclin 1 peptides previously showed an antitumour effect [16], indicating that the introduction of TAT could increase the antitumour potential of

Beclin 1. The HCQ-Lip showed the similar anti-tumour effect with T–B. Consistent with the in vitro results, tumour growth in both the co-treated groups (HCQ plus T–B, HCQ-Lip plus T–B) was significantly impaired compared to the PBS group or T–B group (Fig. 6A). The HCQ plus T–B treatment and HCQ-Lip plus T–B treatment resulted in 62% and 58% reductions, respectively, in the average daily tumour growth rate compared to the PBS-treated controls (18.3 vs. 48.6 mm<sup>3</sup>/day, 20.4 vs. 48.6 mm<sup>3</sup>/day; Fig. 8C). The excised tumour morphology and weights showed 3.3-fold (HCQ-Lip plus T–B vs. T–B) and 2.0-fold (HCQ-Lip plus T–B vs. HCQ plus T–B) tumour growth inhibition, indicating the superiority of the HCQ-Lip plus T–B regimen (Fig. 8B, D). The changes in the body weights of animals were recorded as an indication of safety (Fig. 8E). The body weights of all groups were not significantly different during the treatment, which indicated the low toxicity of our therapeutic regimen. These data show that co-treatment of HCQ-Lip plus T–B had the greatest antitumour effect.

### 3.6. Accumulation of autophagic vesicles in tumour tissue

To determine the mechanism by which autophagy was disrupted in tumours with the different dosing regimens, immunohistochemical analysis and micromorphological study of tumours were performed. After 14 days of treatment, mice were killed and tumour tissues were processed for TEM and immunohistochemistry. Morphologically, the TEM results showed the significant accumulation of autophagic vesicles in HCQ-Lip plus T–B co-treated tumours (Fig. 9A). The increase in LC3

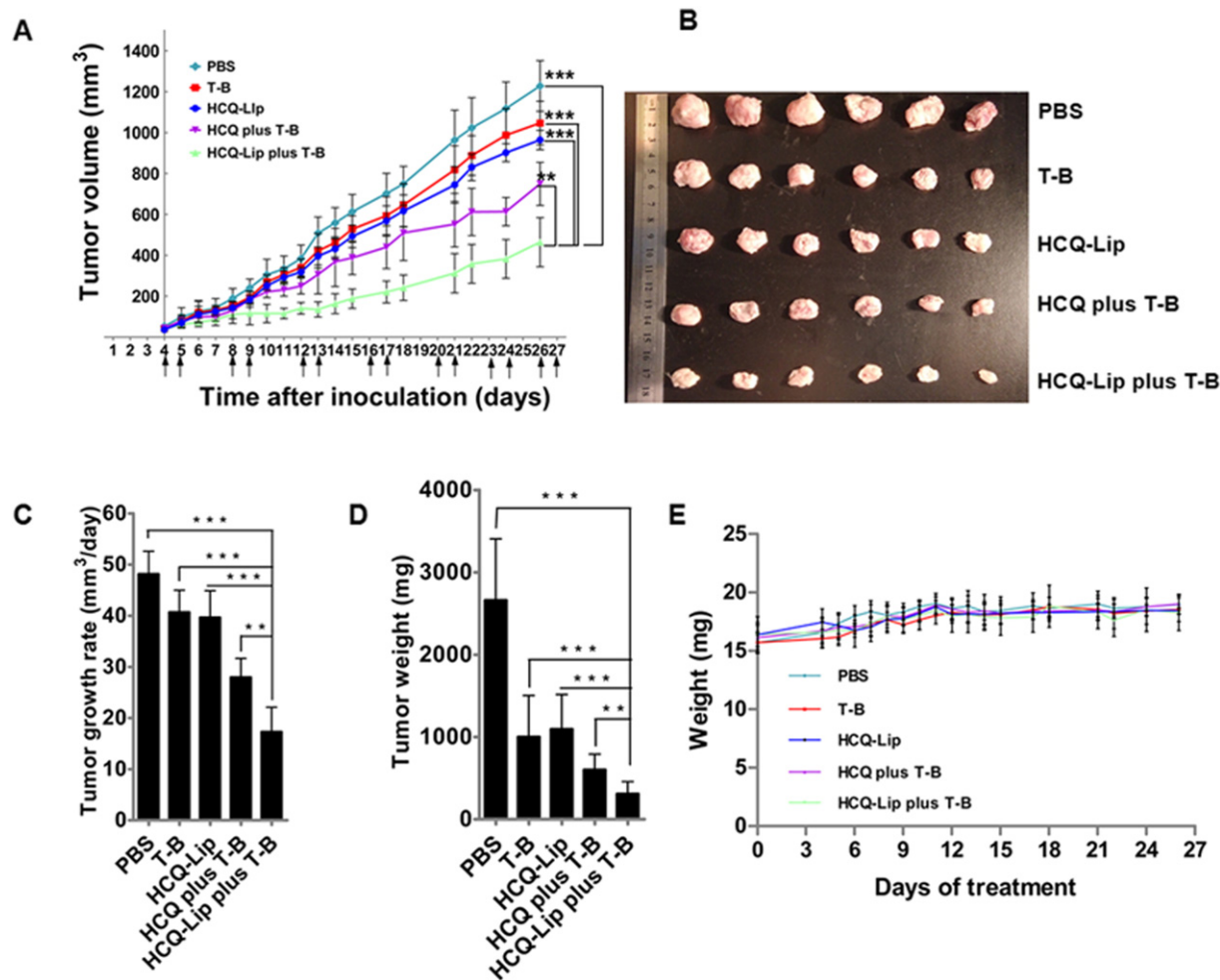


**Fig. 8.** Antitumour assay for HCQ-Lip plus T–B on 4T1 tumour-bearing BALB/C mice. (A) Tumour growth curves of mice receiving different therapeutic regimens as shown ( $n = 6$ , mean  $\pm$  SD). Black arrows indicate times of administration. (B) Photographs of tumours at the end of treatment as indicated. (C) Daily tumour growth rate ( $n = 6$ , mean  $\pm$  SD). (D) Weight of excised tumours ( $n = 6$ , mean  $\pm$  SD). (E) Body weight variations of mice during the treatment. \*\* and \*\*\* indicate  $p < 0.01$  and  $p < 0.001$  versus the compared group, respectively.

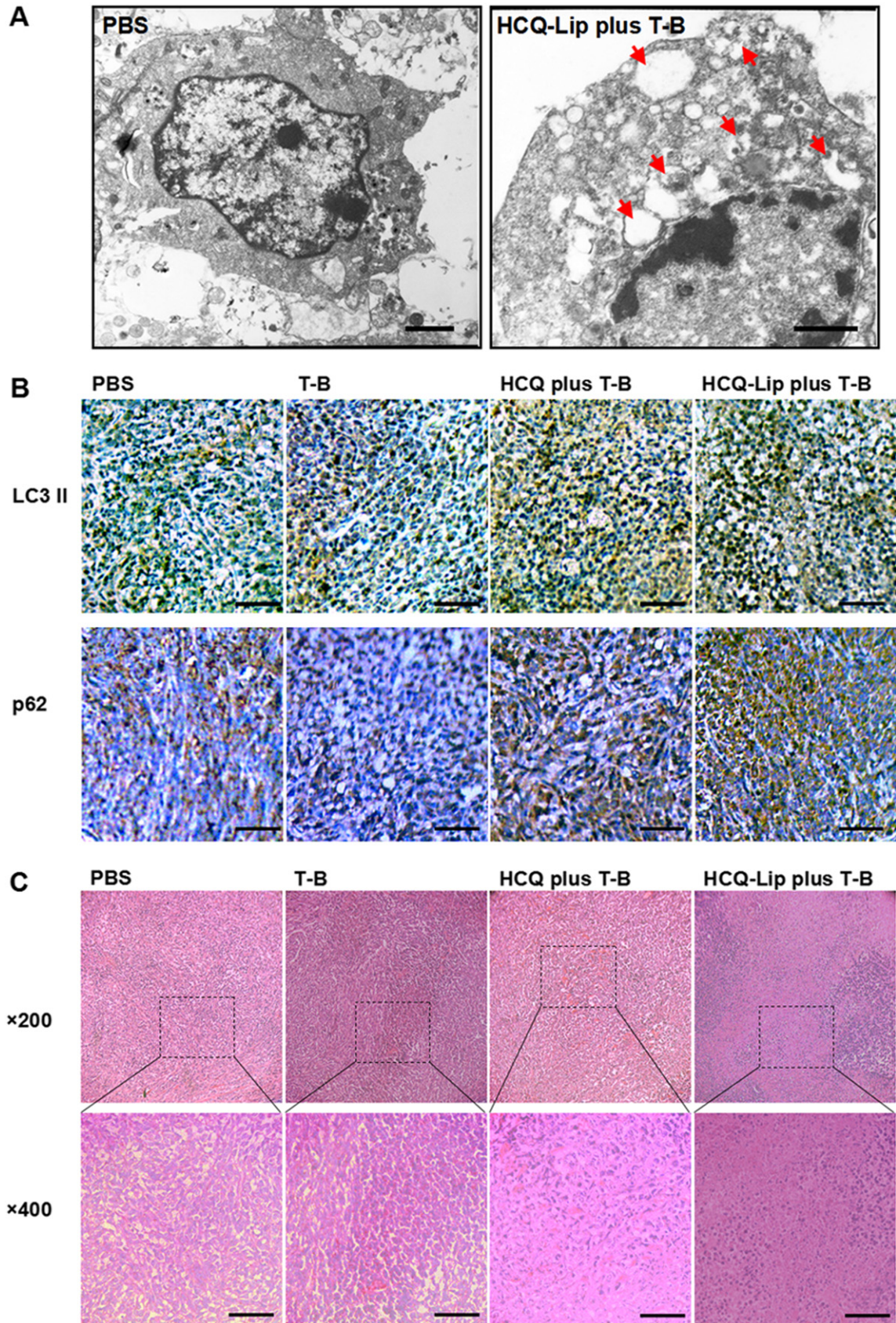


**Fig. 9.** In vivo accumulation of autophagic vesicles and apoptosis and necrosis of inner tumour tissues. (A) Representative electron micrographs of 4T1 xenograft tumours harvested after 14 days of treatment with PBS or HCQ-Lip (65 mg/kg, intravenous injection) plus T-B (1.5 mg/kg, intra-tumoural injection). Arrows: autophagic vesicles. Scale bar: 500 nm. (B) Immunohistochemistry to detect LC3 II and p62 in tumours. Scale bars, 100  $\mu$ m. (C) Haematoxylin and eosin staining of tumour tissues after treatment as indicated. The scale bars represent 100  $\mu$ m.

lipidation in co-treated groups indicated in vivo autophagic accumulation, and the increased p62 in the co-treated group also demonstrated this effect (Fig. 9B). The haematoxylin and eosin staining showed that the autophagy-disrupted tumours exhibited markedly increased apoptotic and, particularly in the centre of the tumours, necrotic areas (Fig. 9C). These studies indicate that the tumour growth inhibition induced by HCQ plus T-B treatment or HCQ-Lip plus T-B treatment is germane to autophagic vacuolisation.

#### 4. Discussion

In various cancer models, autophagy either promotes or inhibits tumour progression depending on the stage and subtype [20]. In this study, the original objective was to explore the relationship between autophagy and cancer cell death; however, we serendipitously observed that the accumulation of autophagosomes in cells is correlative with cell viability and that there is a complex interplay between autophagy, apoptosis, and necrotic signals [30,31]. In some cases, cell apoptosis or necrosis was accompanied by fluctuations in the autophagic flux, with simultaneous changes in regulatory molecular cascades [32,33]. The results presented here suggest that the accumulation of autophagosomes is catastrophic for cells, at least for the cell lines assessed here. Our data reveal that T-B effectively induces autophagic flux in cells, and this may play an important role in phagophore onset. Beclin 1 has an autophagy-inducing function [16], and this CPP grafted autophagy-related peptide was first constructed by Sanae Shoji-Kawata et al. [17]. TAT effectively promotes the cellular uptake of Beclin 1, markedly increasing the autophagy level in cells, which provides therapeutic value for neurodegenerative disorders [19]. We selected this peptide because of its high efficiency and specificity for inducing autophagy in cells. HCQ-Lip has a greater lysosome deacidifying effect than free HCQ, which may be due to the changes in intracellular processes caused by liposomes. Nanometre drug delivery systems are regularly delivered to lysosomes for degradation and detoxification after uptake by cells [34]. Here, the lysosomes were the acting site of HCQ-Lip as hypothesised. When HCQ was released from the liposome into the lysosomes or autolysosomes, its alkalinity impaired the acidic environment and the inner structures, followed by activity changes of the related enzymes. Based on these results, the HCQ-Lip withholds autolysosomes and prevents autophagosome degradation by lysosomal enzymes [35, 36]. The combination of T-B and HCQ-Lip significantly causes cancer cell apoptosis and necrosis, accompanied by the significant aggregation of eGFP-LC3 puncta and an increase in the LC3 II/LC3 I ratio and p62 protein, which together signifies the accumulation of autophagic vesicles. The in vitro cell viability assessment indicated that cell mortality is proportional to the accumulation of autophagic vesicles, which may be because numerous vesicles stimulated the apoptotic and necrotic signal-related pathways [37,38]. Similarly, the in vivo antitumour efficiency of the HCQ-Lip plus T-B co-treated group was notable and occurred with an increase in LC3 II and p62 as evaluated by immunohistochemistry. In addition, the TEM results of the tumour tissues also showed the relationship between autophagic vesicle accumulation and the antitumour effects. In summary, although the detailed mechanism underlying this observation requires further study, our “broadening sources of income and reducing expenditure” style of autophagic flux control in tumour cells embodies its therapeutic antitumour effect.

#### 5. Conclusions

In conclusion, the results presented here reveal a valid antitumour strategy dependent on disrupted autophagic balance in the internal environment of tumour cells. Normally, the autophagic balance in the tumour microenvironment is maintained to ensure tumour progression. However, here, the intracellular accumulation of autophagic vesicles via initiative induction plus the terminal restraint of autophagic flux disturbed the balance and resulted in cell death. Our data reveal that

intracellular autophagic vacuolisation is catastrophic for cells in vitro and tumours in vivo. Our data also demonstrate the antitumour activity of T-B for the first time. The autophagic vacuolisation effect induced by T-B plus HCQ-Lip co-treatment may also be achieved by other reagents or therapeutic regimens.

#### Acknowledgements

The work was funded by the National Natural Science Foundation of China (81373337), the National Basic Research Program of China (973 Program, 2013CB932504) and the State Key Program of National Natural Science of China (81130060).

#### Appendix A. Supplementary data

Supplementary data to this article can be found online at <http://dx.doi.org/10.1016/j.jconrel.2014.12.005>.

#### References

- [1] A.M. Cuervo, E. Bergamini, U.T. Brunk, W. Dröge, M. Ffrench, A. Terman, Review autophagy and aging, *Autophagy* 1 (2005) 131–140.
- [2] A. Kuma, M. Hatano, M. Matsui, A. Yamamoto, H. Nakaya, T. Yoshimori, Y. Ohsumi, T. Tokuhisa, N. Mizushima, The role of autophagy during the early neonatal starvation period, *Nature* 432 (2004) 1032–1036.
- [3] G.E. Mortimore, A.R. Poso, Intracellular protein catabolism and its control during nutrient deprivation and supply, *Annu. Rev. Nutr.* 7 (1987) 539–568.
- [4] B. Levine, J. Yuan, Autophagy in cell death: an innocent convict? *J. Clin. Invest.* 115 (2005) 2679–2688.
- [5] (!!! INVALID CITATION !!!).
- [6] N. Mizushima, B. Levine, A.M. Cuervo, D.J. Klionsky, Autophagy fights disease through cellular self-digestion, *Nature* 451 (2008) 1069–1075.
- [7] J. Debnath, E.H. Baehrecke, G. Kroemer, Does autophagy contribute to cell death? *Autophagy* 1 (2005) 66–74.
- [8] Y. Kondo, T. Kanzawa, R. Sawaya, S. Kondo, The role of autophagy in cancer development and response to therapy, *Nat. Rev. Cancer* 5 (2005) 726–734.
- [9] K.W. Kim, L. Moretti, L.R. Mitchell, D.K. Jung, B. Lu, Combined Bcl-2/mammalian target of rapamycin inhibition leads to enhanced radiosensitization via induction of apoptosis and autophagy in non-small cell lung tumor xenograft model, *Clin. Cancer Res.* 15 (2009) 6096–6105.
- [10] K. Kim, L. Moretti, B. Lu, Combined Bcl(2)/mTOR inhibition leads to enhanced radiosensitization via induction of autophagy and apoptosis in non-small lung tumor xenograft model, *Int. J. Radiat. Oncol.* 72 (2008) S45.
- [11] D. Yang, J. Li, R. Gu, A. Hu, M. Yang, L. Du, X. Zhang, W. Sun, F. Gao, Y. Wu, Myelotomy suppresses autophagic marker LC3-II expression and elevates mTORC1 expression and improves neurological function recovery in rats with spinal cord injury, *Neurol. Asia* 18 (2013).
- [12] A. Kihara, Y. Kabeya, Y. Ohsumi, T. Yoshimori, Beclin–phosphatidylinositol 3-kinase complex functions at the trans-Golgi network, *EMBO Rep.* 2 (2001) 330–335.
- [13] A. Tassa, M. Roux, D. Attaix, D. Bechet, Class III phosphoinositide 3-kinase–Beclin1 complex mediates the amino acid-dependent regulation of autophagy in C2C12 myotubes, *Biochem. J.* 376 (2003) 577–586.
- [14] Q. Sun, W. Fan, K. Chen, X. Ding, S. Chen, Q. Zhong, Identification of Barkor as a mammalian autophagy-specific factor for Beclin 1 and class III phosphatidylinositol 3-kinase, *Proc. Natl. Acad. Sci. U. S. A.* 105 (2008) 19211–19216.
- [15] Z. Yang, D.J. Klionsky, Mammalian autophagy: core molecular machinery and signaling regulation, *Curr. Opin. Cell Biol.* 22 (2010) 124–131.
- [16] X.H. Liang, S. Jackson, M. Seaman, K. Brown, B. Kempkes, H. Hibshoosh, B. Levine, Induction of autophagy and inhibition of tumorigenesis by beclin 1, *Nature* 402 (1999) 672–676.
- [17] S. Shoji-Kawata, R. Sumpter, M. Leveno, G.R. Campbell, Z. Zou, L. Kinch, A.D. Wilkins, Q. Sun, K. Pallauf, D. MacDuff, Identification of a candidate therapeutic autophagy-inducing peptide, *Nature* 494 (2013) 201–206.
- [18] M. Rosenfeld, S. Brem, T. Mikkelsen, D. Wang, S. Piao, L. Davis, P. O'Dwyer, R. Amaravadi, Pharmacokinetic analysis and pharmacodynamic evidence of autophagy inhibition in patients with newly diagnosed glioblastoma treated on a phase I trial of hydroxychloroquine in combination with adjuvant temozolomide and radiation (ABTC 0603), *J. Clin. Oncol.* 28 (2010) 3086.
- [19] K. Maruyama, Intracellular targeting delivery of liposomal drugs to solid tumors based on EPR effects, *Adv. Drug Deliv. Rev.* 63 (2011) 161–169.
- [20] K.S. Choi, Autophagy and cancer, *Exp. Mol. Med.* 44 (2012) 109–120.
- [21] E.C. Freundt, M. Czapiaga, M.J. Lenardo, Photoconversion of LysoTracker Red to a green fluorescent molecule, *Cell Res.* 17 (2007) 956–958.
- [22] S. Kimura, T. Noda, T. Yoshimori, Dissection of the autophagosome maturation process by a novel reporter protein, tandem fluorescent-tagged LC3, *Autophagy* 3 (2007) 452.
- [23] S. Sarkar, E.O. Perlstein, S. Imarisio, S. Pineau, A. Cordenier, R.L. Maglathlin, J.A. Webster, T.A. Lewis, C.J. O'Kane, S.L. Schreiber, Small molecules enhance autophagy and reduce toxicity in Huntington's disease models, *Nat. Chem. Biol.* 3 (2007) 331–338.

- [24] Y. Kabeya, N. Mizushima, T. Ueno, A. Yamamoto, T. Kirisako, T. Noda, E. Kominami, Y. Ohsumi, T. Yoshimori, LC3, a mammalian homologue of yeast Apg8p, is localized in autophagosomal membranes after processing, *EMBO J.* 19 (2000) 5720–5728.
- [25] I. Tanida, T. Ueno, E. Kominami, LC3 conjugation system in mammalian autophagy, *Int. J. Biochem. Cell Biol.* 36 (2004) 2503–2518.
- [26] G. Bjørkøy, T. Lamark, A. Brech, H. Outzen, M. Perander, A. Øvervatn, H. Stenmark, T. Johansen, p62/SQSTM1 forms protein aggregates degraded by autophagy and has a protective effect on huntingtin-induced cell death, *J. Cell Biol.* 171 (2005) 603–614.
- [27] S. Pankiv, T.H. Clausen, T. Lamark, A. Brech, J.-A. Bruun, H. Outzen, A. Øvervatn, G. Bjørkøy, T. Johansen, p62/SQSTM1 binds directly to Atg8/LC3 to facilitate degradation of ubiquitinated protein aggregates by autophagy, *J. Biol. Chem.* 282 (2007) 24131–24145.
- [28] R. Mathew, C.M. Karp, B. Beaudoin, N. Vuong, G. Chen, H.Y. Chen, K. Bray, A. Reddy, G. Bhanot, C. Gelinas, R.S. D'Alpaola, V. Karantza-Wadsworth, E. White, Autophagy suppresses tumorigenesis through elimination of p62, *Cell* 137 (2009) 1062–1075.
- [29] M. Van Engeland, L.J. Nieland, F.C. Ramaekers, B. Schutte, C.P. Reutelingsperger, Annexin V-affinity assay: a review on an apoptosis detection system based on phosphatidylserine exposure, *Cytometry* 31 (1998) 1–9.
- [30] J. Moscat, M.T. Diaz-Meco, p62 at the crossroads of autophagy, apoptosis, and cancer, *Cell* 137 (2009) 1001–1004.
- [31] S. Shen, O. Kepp, M. Michaud, I. Martins, H. Minoux, D. Metivier, M. Maiuri, R. Kroemer, G. Kroemer, Association and dissociation of autophagy, apoptosis and necrosis by systematic chemical study, *Oncogene* 30 (2011) 4544–4556.
- [32] R.T. Marquez, L. Xu, Bcl-2:Beclin 1 complex: multiple mechanisms regulating autophagy/apoptosis toggle switch, *Am. J. Cancer Res.* 2 (2012) 214.
- [33] I. Tanida, T. Ueno, E. Kominami, LC3 and autophagy, *Autophagosome and Phagosome*, Springer, 2008, pp. 77–88.
- [34] V.P. Torchilin, Recent advances with liposomes as pharmaceutical carriers, *Nat. Rev. Drug Discov.* 4 (2005) 145–160.
- [35] S.P. Sundelin, A. Terman, Different effects of chloroquine and hydroxychloroquine on lysosomal function in cultured retinal pigment epithelial cells, *APMIS* 110 (2002) 481–489.
- [36] R.I. Fox, Mechanism of action of hydroxychloroquine as an antirheumatic drug, *Seminars in Arthritis and Rheumatism*, Elsevier, 1993, pp. 82–91.
- [37] A.L. Edinger, C.B. Thompson, Death by design: apoptosis, necrosis and autophagy, *Curr. Opin. Cell Biol.* 16 (2004) 663–669.
- [38] S.L. Fink, B.T. Cookson, Apoptosis, pyroptosis, and necrosis: mechanistic description of dead and dying eukaryotic cells, *Infect. Immun.* 73 (2005) 1907–1916.